Tuning hole charge collection efficiency in polymer photovoltaics by optimizing the work function of indium tin oxide electrodes with solution-processed LiF nanoparticles

Hasan Kurt, Junjun Jia, Yuzo Shigesato & Cleva W. Ow-Yang

Journal of Materials Science: Materials in Electronics

ISSN 0957-4522
Volume 26
Number 11

J Mater Sci: Mater Electron (2015)
26:9205-9212
DOI 10.1007/s10854-015-3613-z

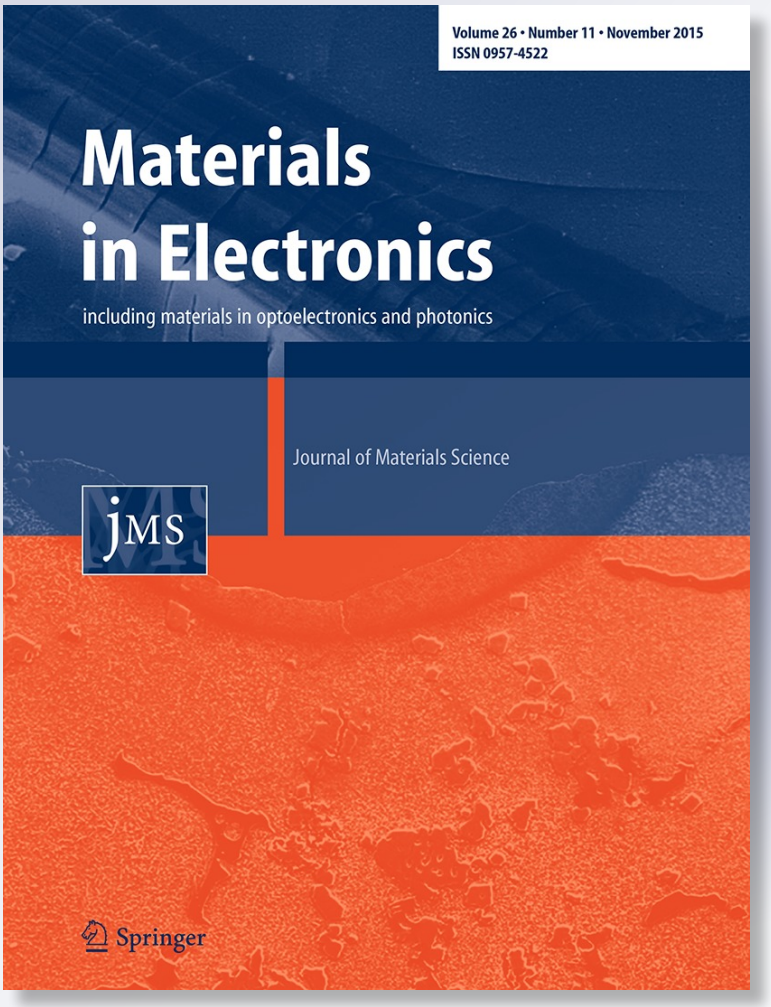

Springer

J Mater Sci: Mater Electron (2015) 26:9205–9212
DOI 10.1007/s10854-015-3613-z

Tuning hole charge collection efficiency in polymer photovoltaics by optimizing the work function of indium tin oxide electrodes with solution-processed LiF nanoparticles

Hasan Kurt[1] · Junjun Jia[2] · Yuzo Shigesato[2] · Cleva W. Ow-Yang[1,3]

Received: 21 April 2015 / Accepted: 8 August 2015 / Published online: 13 August 2015

Abstract By varying the density of solution-processed lithium fluoride (sol-LiF) nanoparticles at the interface between tin-doped indium oxide (ITO) and poly(3,4-ethylenedioxythiophene):poly(styrenesulfonate) (PEDOT:PSS), we have demonstrated that the electronic hole collection efficiency of an organic photovoltaic cell can be optimized through tuning the energy level alignment at the ITO/PEDOT:PSS interface. We synthesized the LiF nanoparticles in solution and deposited them onto ITO electrodes with increasing surface coverage up to 13.2 %. The surface work function of the nanostructured ITO increased linearly from 4.88 to 5.30 eV. When the sol-LiF-modified ITO electrodes were incorporated into polymer solar cells based on a bulk heterojunction of poly(3-hexylthiophene) polymer and methanofullerene, a maximum power conversion efficiency was recorded for a device with an ITO anode modified by 5.3 % of sol-LiF coverage, which corresponded to a measured work function of 5.07 eV. The improvement in short circuit current density by 87 % and power conversion efficiency by 74.3 % suggest that the sol-LiF interlayer density enabled work function tuning of the ITO anode to better match the highest occupied molecular orbital level of PEDOT:PSS, facilitating hole charge collection. The increase in electronic hole collection efficiency is attributed to both a lowered resistance at the ITO modified by sol-LiF and faster hole transport, although these gains are offset by an associated increase in contact polarization. Our findings suggest that the surface work function of ITO can be tuned to improve energy level alignment with other contact layers via the surface density of sol-LiF particles. More efficient hole transport, due to higher recombination resistance, offset by an increased charge extraction barrier presented by contact polarization; the two effects combined give rise to an optimum in sol-LiF nanostructuring of the ITO surface properties.

Electronic supplementary material The online version of this article (doi:10.1007/s10854-015-3613-z) contains supplementary material, which is available to authorized users.

✉ Cleva W. Ow-Yang
cleva@sabanciuniv.edu

[1] Faculty of Engineering and Natural Sciences, Sabanci University, Orhanli, Tuzla, 34956 Istanbul, Turkey

[2] Graduate School of Science and Engineering, Aoyama Gakuin University, 5-10-1 Fuchinobe, Chuo, Sagamihara 252-5258, Japan

[3] Nanotechnology Research and Application Center, Sabanci University, Orhanli, Tuzla, 34956 Istanbul, Turkey

1 Introduction

Organic photovoltaics (OPV) have competitive potential for harvesting solar energy, due to their adaptability for low-cost, solution-based, roll-to-roll (R2R) production of large-area, flexible, and ultimately portable, devices [1, 2]. While the initial targets set for commercializability of polymer-based bulk heterojunction (BHJ) OPV devices—power conversion efficiencies of 10 % [3] and stability over 10 years [4]—have been met with the development of new active layers and device architectures, further performance enhancement and stability can be realized by engineering the interfaces between the different functional layers, such as at the electrode, for reduced traps sites, better energy level alignment, improved charge extraction, superior wettability and interfacial compatibility and optimized surface work functions [5].

Due to the low compatibility between intrinsically different structures at the molecular level, organic–inorganic interfaces often result in recombination losses due to low charge carrier mobility and limited charge carrier lifetimes [6]. By improving matching of the electronic structure at the low work function (Φ) electrode interface, mobile hole extraction can be increased, thereby lowering recombination losses and enhancing the electronic hole contribution to the current density. In this context, the surface energy and Φ of the electrode, typically of tin-doped indium oxide (ITO) in conventional BHJ device architectures, are key factors determining the overall device performance.

To tune the properties of the electrode/active layer interface, a panoply of approaches have been adopted [7]—self-assembled monolayers [8–10], and chlorine surface modification [11]; organic layers [12–14]; carbon-based nanomaterials [15, 16]; transition-metal oxides [17–21]; and alkali halides such as CsF and LiF [22]. Interlayer engineering (IE) enables not only the tuning of charge collection efficiency and charge selectivity on both electrodes, but also control over OPV stability and durability. An additional parameter for tuning at the high Φ electrode is PEDOT:PSS, which is commonly used as an electronic hole transport/electron-blocking layer. Considering the low electronic homogeneity [23] and the low-pH nature of PEDOT:PSS, the interface it forms with ITO offers limited electron-blocking capability [24], as well as chemical instability leading to Indium diffusion into active layers [25]. The scope of our study reported herein is focused on interface engineering of the ITO/PEDOT:PSS interlayer in P3HT:PCBM BHJ photovoltaic devices, through tuning charge collection efficiency by nanostructuring, and *in-operando* analysis elucidating the relevant mechanisms.

Impedance spectroscopy (IS) is a non-destructive small perturbation technique for monitoring the dynamics in an electrochemical system. Recently, this technique has been applied toward probing photoelectrochemical response in organic photovoltaics. [26] In IS, low amplitude alternating current (AC) signal is applied to probe charge carrier dynamics, recombination kinetics, diffusion mechanisms and the density of states in both in situ and dark conditions. The Cole–Cole plots of OPVs typically consist of a dominant semi-circle arc at low frequencies, associated with the recombination of photogenerated charge carriers within active layers. At higher frequencies, transport and series resistances determine the impedance behavior, in addition to the dielectric response.

The measured capacitance in OPVs consists of multiple contributions: (1) the geometrical capacitance, which arises from the depletion layer between the opposing electrodes, and (2) the chemical capacitance, which can also be thought of as the electrochemical potential originating from photogenerated charge carriers at BHJ interfaces [26]. In order to analyze the individual OPV operating mechanisms, several different forms of equivalent circuit models have been proposed [27]. IS enables the evaluation of BHJs, interlayers and interfaces in terms of their individual roles and impacts in OPV operation, such as charge extraction efficiency, charge transport efficiency, global charge mobility, recombination and trap assisted losses.

Previously, we have reported the development of solution-processed LiF (sol-LiF) nanoparticles for bottom-up assembly of the LiF interlayer at the ITO electrode [28], a consequent increase in surface Φ, and a substantial increase in power conversion efficiency (PCE) and short circuit current density (J_{sc}) in a conventional ITO/sol-LiF/PEDOT:PSS/P3HT/PC60BM/thermal-LiF/Al OPV [29]. Moreover, we have observed that varying the surface coverage of sol-LiF nanoparticles offer additional tunability for the ITO surface Φ, suggesting that device performance can be tailored by tuning the energy level alignment at the organic–inorganic interface [30]. In this manuscript, we report a study of the correlation between sol-LiF surface coverage and P3HT:PCBM BHJ OPV performance.

2 Materials and methods

We synthesized LiF nanoparticles (sol-LiF) using reverse diblock copolymer (DBCP) micelles suspended in toluene [28]. The sol-LiF-loaded DBCP micelle solution was deposited by spin-coating onto cleaned (sonicating for 10 min in successively acetone, methanol, isopropanol) indium tin oxide (ITO) thin film-coated substrates (Thin Film Devices Eagle XG, Anaheim, CA, USA) at 2000 rpm. The polymeric micelle material was removed by etching with an oxygen plasma (Harrick Plasma PDC-002, Ithaca, NY, USA) at 29.6 W, 950 mTorr conditions for 90 min. The sol-LiF surface coverage on the substrates was varied by sequentially spin-coating and oxygen plasma, cycling 1, 3, 5, 7 and 10 times. For evaluating nanoparticle characteristics, we also deposited identical sol-LiF layers onto Si substrates (University wafer #444, Boston, MA, USA) and imaged the resulting nanostructure dispersions in the scanning electron microscope (SEM, Leo Supra 35VP, Oberkochen, Germany). Using ImageJ [31], we quantified the surface coverage and interparticle distance by performing spatial point pattern analysis on the SEM micrographs. To determine the root mean square (RMS) surface roughness, we carried out topographical analysis using an atomic force microscope (AFM, Bruker Multimode 8 with a high resolution E-type piezo-scanner head, Santa Barbara, CA, USA). To analyze the work function, Φ, of the sol-LiF-modified and unmodified ITO surfaces, we performed photoelectron spectroscopy in air (PESA, Riken Keiki Co. Ltd. AC-2, Tokyo, Japan).

We integrated the sol-LiF interlayers into conventional poly(3-hexylthiophene-2,5-diyl:[6,6]-phenyl-C_{61}-butyric acid methyl ester (P3HT:PCBM) BHJ devices. Pre-patterned indium tin oxide anode substrates (ITO, Ossila S101, Sheffield, UK) with and without sol-LiF nanoparticles were sonicated in acetone, methanol and isopropanol baths for 10 min each, before 30 min of UV–ozone treatment. A thin layer of diluted poly(3,4-ethylenedioxythiophene):polystyrene sulfonate (PEDOT:PSS, Heraeus Clevios^{TM} P VP AI 4083, filtered at 0.45 μm) was deposited by spin-coating (5000 rpm, ~40 nm thickness) and annealed at 150 °C for 15 min. P3HT (Ossila M102, Sheffield, UK; M_w 65200, RR 95.7 %) and $PC_{60}BM$ (Ossila M111, Sheffield, UK; 99 %) were mixed in a 1:0.6 weight ratio in chlorobenzene. P3HT:$PC_{60}BM$ (25 mg/mL) solution was deposited by spin-coating at 2000 rpm for 60 s, resulting in a ~90 nm thick layer. Layer thicknesses were measured using a surface profiler (KLA-Tencor P6, Milpitas, CA, USA). The samples were thermally annealed at 150 °C for 10 min and immediately transferred to a thermal evaporator chamber and placed under high vacuum ($<\sim 2 \times 10^{-6}$ mbar). To make the back-side electrical contact, we performed thermal evaporation of a 1.2 nm-thick LiF layer, followed by a 100 nm-thick Al cathode layer on the organic active layers. The samples were then annealed at 150 °C for 10 min after cathode evaporation. The devices were subsequently encapsulated using UV-curable epoxy (Ossila E131, Sheffield, UK).

The final device structure produced was composed of the following layer sequence: ITO/sol-LiF interlayer/PEDOT:PSS/P3HT:PCBM/LiF/Al, where the sol-LiF interlayer was deposited by sequentially spin-coating and plasma etching 1, 3, 5, 7 and 10 times. The device size for each cell was 0.045 cm. We measured the current density–voltage (J–V) characteristics using a source meter (Keithley Instruments Model 2400, Cleveland, OH, USA) under AM 1.5G solar irradiation at 100 mW/cm^2 (Newport Corporation Oriel Sol3A Class AAA 91192 Solar Simulator equipped with 450 W xenon lamp, Newport, CA, USA). The light intensity was calibrated by reference Si photodiode cell.

To analyze the charge transport and recombination dynamics in devices based on ITO modified by sol-LiF, we conducted impedance measurements using a Solartron 1260 Impedance/Gain-phase Analyzer equipped with a Solartron 1286 Dielectric Interface. We measured an impedance response over the range of 0.1 Hz–1 MHz with an oscillation amplitude of 10 mV, as well as under dark and illuminated conditions over a DC bias range of −1 to 1 V and of 0–0.75 V respectively. We used a halogen lamp at ~100 mW/cm^2 to illuminate the devices. For each device, the illumination intensity was set by adjusting the lamp such that the device exhibited the same short circuit current (I_{sc}) that was measured under AM1.5G illumination. Measurements at reduced illumination were realized by using neutral density filters. Finally, we optimized the equivalent circuit modeling using ZView and EIS Spectrum Analyzer software [32].

3 Results

A single layer of sol-LiF deposited on ITO substrates showed quasi-hexagonal ordering in the nanoparticle dispersion, due to a highly monodisperse DBCP micelle size, as shown in Fig. 1. The average sol-LiF diameter was 9 ± 2.7 nm, while the average interparticle distance was 70.1 ± 12.2 nm. Sequential spin-coating of sol-LiF nanoparticles and oxygen plasma treatments yielded a linear increase in surface coverage by sol-LiF on ITO substrates, as shown in Fig. 2. The sol-LiF layer introduced roughness on the ITO surface. For a single sol-LiF deposition, we measured a surface roughness of 2.3 nm, while three cycles of sequential spin-coating and etching increased the surface roughness to an RMS of 5.0 nm. Further sequential spin-coating steps increased the surface roughness less dramatically, reaching a maximum RMS of 7.2 nm for 10 iterations.

The Φ of sol-LiF-modified ITO increased with the sol-LiF surface coverage, as shown in Fig. 2a. Bare ITO substrates were exposed to an oxygen plasma treatment of the same duration and conditions as substrates with a single sol-LiF deposition and had a measured work function of 4.88 eV. To tune the Φ of the ITO surface by controlling the ITO surface coverage by sol-LiF, we carried out a sequential alternation of sol-LiF-loaded micelle deposition and etch removal up to 10 times (i.e., 13.2 % coverage), modifying Φ up to 5.30 eV.

We incorporated the sol-LiF nanostructured ITO surfaces into conventional P3HT:PCBM BHJ photovoltaic devices. The control devices consisted of the standard

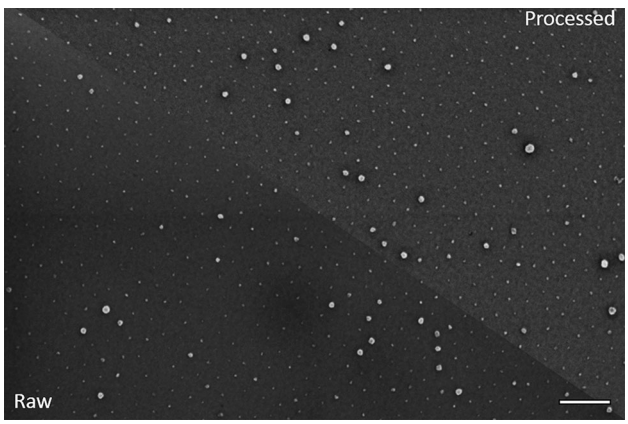

Fig. 1 Raw and processed SEM micrograph of single sol-LiF deposition, 2 % surface coverage. *Scale bar* represents 200 nm

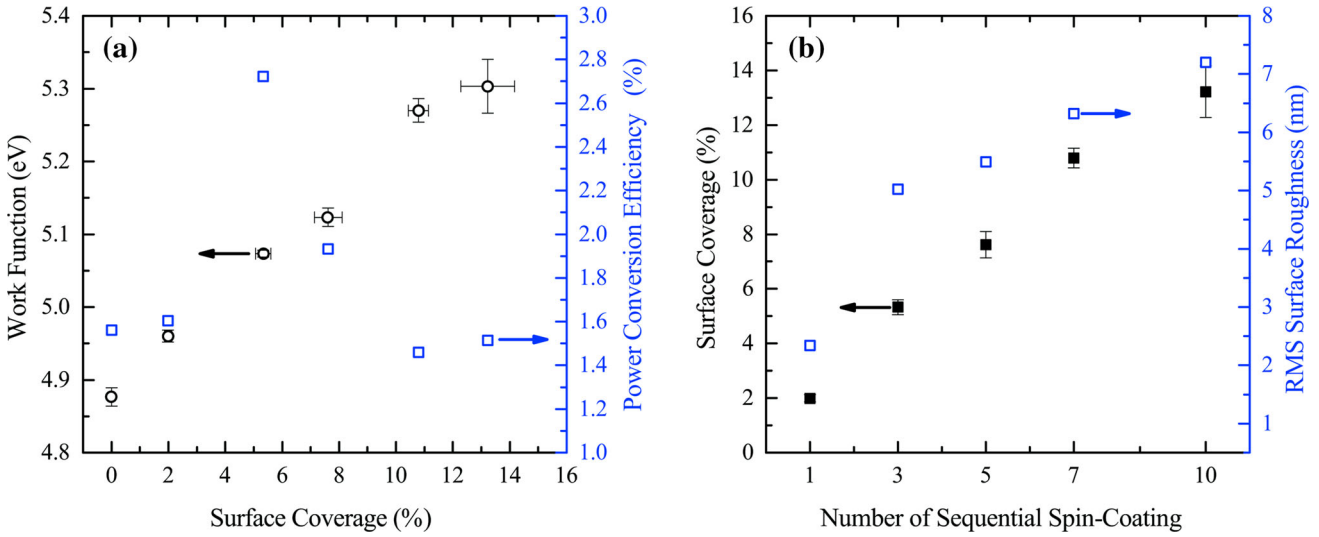

Fig. 2 **a** Correlation between work function modification and power conversion efficiency of P3HT:PC60BM devices with sol-LiF coverage on ITO; **b** correlation between sol-LiF surface coverage and surface roughness of sol-LiF modified ITO with sequential spin-coating steps

PEDOT:PSS layer deposited on top of ITO without sol-LiF, and the PCE measured was 1.51 ± 0.11 %, based on 12 devices. When the ITO was modified by 5.3 % sol-LiF coverage, the best power conversion efficiency (PCE) had improved to 2.7 %, corresponding to a 74.3 % improvement over the control device. For the OPV containing an ITO anode modified by 7.6 % sol-LiF coverage, the PCE was 23.7 % higher than the best control device.

The *J*–*V* characteristics are summarized in Fig. 3. The device with ITO modified by 5.3 % sol-LiF coverage showed a short circuit current density (J_{sc}) of 13.2 mA/cm^2, which is a substantial 87 % improvement. In devices with other sol-LiF coverages, J_{sc} fell within a narrow range of 1–4 % improvement. The key parameters of OPVs with ITO anodes modified by different coverages of sol-LiF were tabulated in Table 1. The open circuit voltages (V_{oc}) were similar for the control and sol-LiF-containing OPVs—the variation in values fell within the limits of measurement error. While the fill factor (FF) for control devices was extracted to be 45 %, OPVs with sol-LiF deposited ITO anodes dropped to the 42–44 % regime, with the exception of the device containing ITO covered 7.6 % by sol-LiF, for which the FF improved to 48.2 %.

The shunt resistance, generally associated with leakage currents in the device [29], and parasitic series resistance (R_s) were extracted using the diode model under constant 1

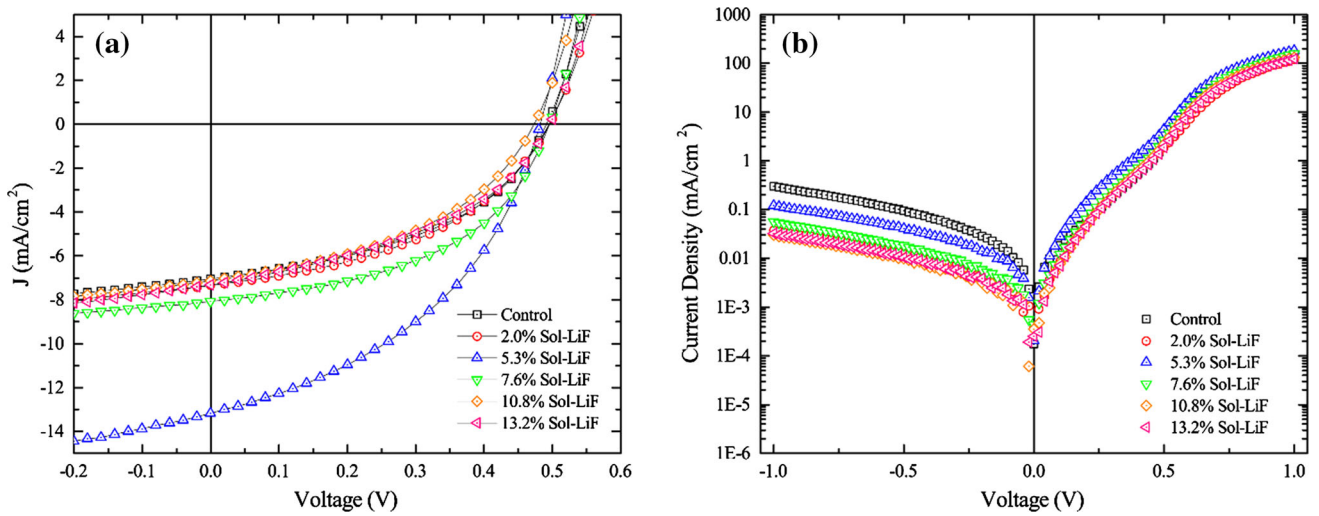

Fig. 3 Current density–voltage characteristic curves of P3HT:PC60BM solar cells with ITO anodes modified by different sol-LiF surface coverages, **a** under AM1.5G illumination; **b** in the dark

Table 1 The key parameters of OPVs with different levels of LiF nanostructured ITO anodes under AM1.5G illumination

LiF NP surface coverage (%)	Work function of nanostructured ITO surface	V_{oc} (mV)	J_{sc} (mA/cm^2)	FF (%)	Best PCE (%)	Dark ideality factor	J_{sat} (mA/cm^2)	R_s (Ω/cm^2)	R_{sh} (Ω/cm^2)	Average PCE (%)
0	4.88	492	7.04	45.0	1.56	1.89	7.8E−8	2.23	543.6	1.51 ± 0.11
2.0	4.96	495	7.34	44.1	1.60	2.07	12.5E−8	2.07	716.8	1.57 ± 0.02
5.3	5.07	482	13.17	42.8	2.72	1.73	5.2E−8	1.77	282.3	2.59 ± 0.15
7.6	5.12	496	8.06	48.2	1.93	1.84	7.0E−8	1.90	739.8	1.84 ± 0.07
10.8	5.27	473	7.12	43.2	1.46	1.90	8.5E−8	2.20	590.9	1.45 ± 0.01
13.2	5.30	496	7.31	41.7	1.51	1.94	9.3E−8	2.27	730.4	1.47 ± 0.03

Average PCE was obtained from measurements of the best six performing devices

sun illumination [33]. The dark current ideality factor (n) and reverse saturation current density (J_{sat}) were extracted from dark J–V characteristics according to the two-diode model developed by Suckow et al. [33]. Although R_s had increased only in the device with 13.2 % sol-LiF coverage, it was reduced in the other devices, with the best improvement being 21 and 15 % of R_s in the control devices, for those with 5.3 and 7.6 % sol-LiF coverage, respectively. The shunt resistance (R_{shunt}) of the control devices was 589 ± 54 Ω/cm^2. The device containing the 5.3 % sol-LiF-modified ITO anode showed an R_{shunt} 48 % lower than the control devices, whereas the devices with other sol-LiF coverages all had R_{shunt} values 22–26 % better. While the control devices demonstrated an n of 1.89, ITO electrodes with 5.3 and 7.6 % sol-LiF coverage demonstrated improved n values of 1.73 and 1.84 respectively. In parallel with ideality factors, J_{sat} were slightly improved from 7.8 × 10^{-8} to 5.2 × 10^{-8} mA/cm^2 and to 7.0 × 10^{-8} mA/cm^2, respectively for 5.3 and 7.6 % sol-LiF covered ITO anodes.

In order to obtain further insight into the charge carrier dynamics in the device structure, we evaluated the impedance response of the devices with nanostructured ITO during operation (Fig. 4) and summarize the results of the response analysis in Table 2. Analysis of the Cole–Cole plots [26] revealed that the contact resistance (R_{co}) was reduced by 78 and 76 %, when ITO was modified by 5.3 and 7.6 % sol-LiF surface coverage, respectively, which was also associated with a corresponding increase in the contact polarization (C_{co}) by 42 and 43 %. For analyzing recombination in the BHJ, we applied the constant phase element (CPE) method. In general, the sol-LiF nanostructuring significantly improved recombination resistance (R_2) and led to improvement in the average recombination time (τ_{ave}) by up to sixfold. The bulk resistance (R_1), comprising of the resistance from all layers between the electrodes, increased significantly in comparison to control devices.

4 Discussion

To understand why the conventional P3HT:PCBM (1:0.6) devices, which were fabricated in ambient air and clean room conditions, showed a substantial 74.5 % improvement in PCE when the ITO anode was modified by 5.3 % sol-LiF coverage, it would be worthwhile to revisit Fig. 2a and note that these modified anodes had a surface Φ of 5.07 eV. The modified anode with such a Φ value would align well with the energy level of PEDOT:PSS, reported to be at 5.10 eV [34, 35]. As depicted in Fig. 5, it appears that the Φ of the modified ITO facilitates the collection of hole charges through reducing the Schottky barrier between ITO and PEDOT:PSS to an ohmic contact. The better energy level alignment thus contributes to the 87 % improvement in J_{sc}. As J_{sc} indicates the number of photogenerated charge carriers extracted to the external circuit, these results are consistent with an improvement in hole collection efficiency.

Since faster and improved charge collection efficiency would be due to an increase in the effective charge carrier lifetime within the BHJ, we used impedance spectroscopy to gain insight into the *in-operando* charge carrier dynamics. The results revealed a general improvement in the effective charge carrier lifetime up to sixfold, correlated with a 78 % decrease in contact resistance in the best-performing device. Since hole mobility and thickness in the PEDOT:PSS hole transport layer were not changed, the faster hole transport—viz., through increased recombination resistance R_2 and increased recombination lifetime τ_{avg}—can be attributed to the increased electronic surface states at the modified ITO [28, 30], resulting in an increase electrical potential gradient imposed on the mobile holes and sweeping them to the anode more quickly. However, the hole collection efficiency and short circuit current improvement were still significantly below what this improvement leads us to expect. One possible explanation would be that the increase in induced polarization at the

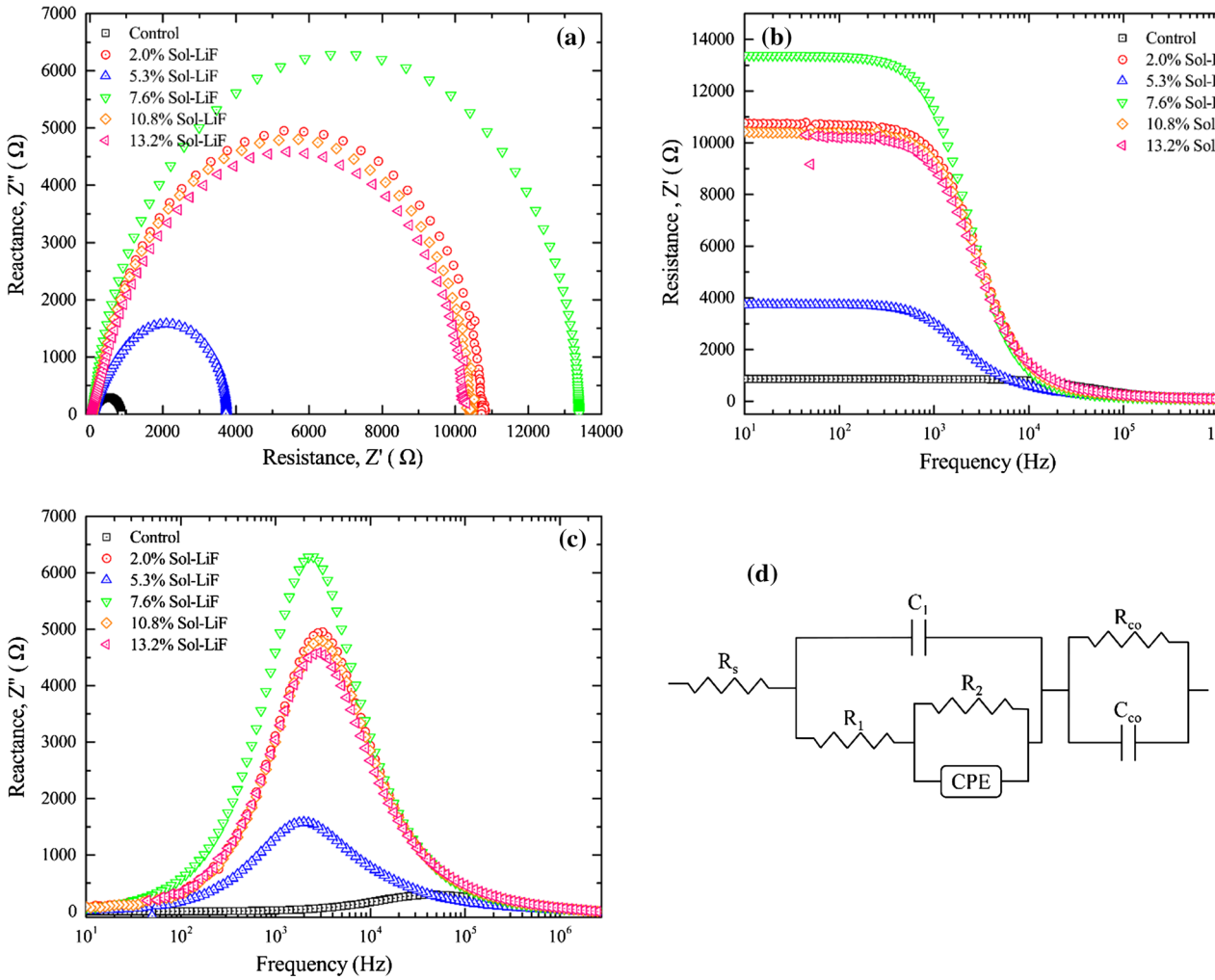

Fig. 4 Impedance response of OPVs with 5 different percentages of sol-LiF nanostructuring modifying the ITO electrode, compared to a control device, all under 1 sun illumination (**a**–**c**), and the corresponding equivalent circuit model **d**

Table 2 Extracted equivalent circuit components under 1 sun illumination

LiF NP surface coverage (%)	Φ of nanostructured ITO surface	R_{Co} (Ω)	C_{co} (nF)	R_1 (kΩ)	C_1 (nF)	R_2 (kΩ)	Q, magnitude of CPE (nF)	N, ideality of CPE	C_{eq} (nF)	τ_{ave} (μs)	Average PCE (%)
0	4.88	395.6	7.87	0.194	4.11	0.175	45.21	1	45.21	7.93	1.51 ± 0.11
2.0	4.96	99.2	6.42	3.315	3.82	7.326	10.05	0.86	2.17	15.94	1.57 ± 0.02
5.3	5.07	86.9	11.14	1.331	12.60	2.256	39.47	0.93	21.21	47.89	2.59 ± 0.15
7.6	5.12	96.3	11.24	7.410	4.26	5.793	9.56	0.91	3.66	21.22	1.84 ± 0.07
10.8	5.27	108.6	7.64	3.391	3.90	6.914	9.42	0.87	2.45	16.95	1.45 ± 0.01
13.2	5.30	114.7	6.68	2.677	3.67	7.443	11.41	0.87	3.12	23.26	1.47 ± 0.03

ITO contact surface would offset these gains, leading to a charge accumulation in sol-LiF interface. The tradeoff between the competing effects [26] gives rise to the optimal device PCE of 2.59, when 5.3 % of the ITO surface is modified by sol-LiF nanostructuring.

Furthermore, contributions to R_s can come from three sources: (1) contact resistance between the electrode and the active layer, (2) the bulk resistance of the polymer film, or (3) the bulk resistance of the contacts [36]. In this study, the polymer film and the contacts were the same for all of

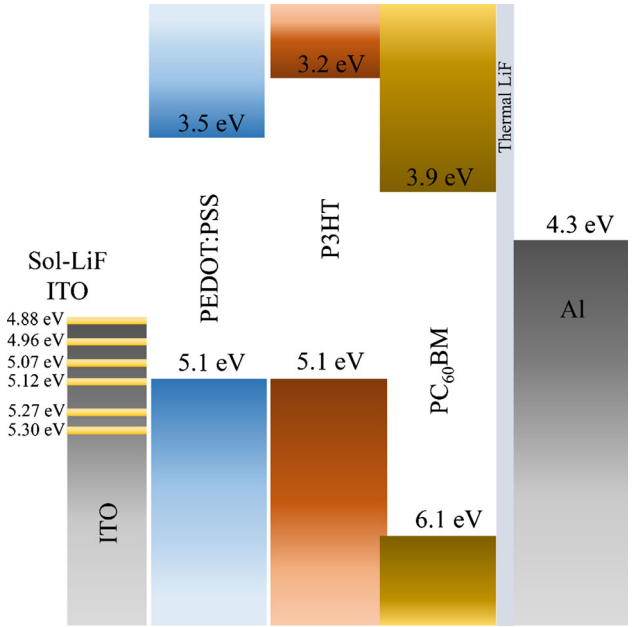

Fig. 5 Schematic of energy level alignment of ITO anodes modified by sol-LiF in the P3HT:PCBM device architecture

the devices tested, so the variation in R_s stems from differences at the contact between the electrode and the active layer, i.e. with sol-LiF coverage [29]. When sol-LiF NPs increase the modified ITO surface Φ, the charge transfer away from the ITO is increased into the dielectric layer in direct contact [28]. Thus with little variation in electrical potential at the contact and an increase in the charge collection current for the modified electrode with the 5.07 eV work function, it follows that the contact resistance for the device with this interlayer would be the lowest. For ideal solar cell behavior, R_s should be 0 and R_{shunt} infinite [36].

Reduction in J_{sat} and n parameters could be the indicator of greater selectivity in harvesting charge carriers [19]. This enhancement can be attributed to lowering the energy barrier for hole charge carrier [37] and reduced surface recombination for bound-polaron pairs [38, 39] at the PEDOT:PSS/ITO interface.

Compared to the control device, the low R_{shunt} for the device with Φ of 5.07 eV suggests a difference in wetting by the PEDOT:PSS layer. From Fig. 2, the modified ITO surface roughness scaled directly proportional to sol-LiF surface coverage. An increase in surface roughness could lead to the formation of hot spots in the electrode layer. However, sol-LiF modified ITO anodes either improved or did not affect R_{shunt} with the exception of 5.3 % sol-LiF coverage. Moreover, increasing surface roughness increased R_s with respect to control devices with the exception of 13.2 % sol-LiF coverage.

In addition to roughness, discontinuity in the sol-LiF layer may also induce changes in wetting of PEDOT:PSS on the modified electrode. However, SEM images of all layers reveal sol-LiF layers which are discontinuous for all surface coverages investigated [30], the discontinuous nature of the sol-LiF layer would not be the root cause for the unusually low R_{shunt} relative to the other devices with unmodified and modified ITO electrodes.

Despite the dramatic improvement in J_{sc} and R_s for the modified electrode with a Φ of 5.07 eV, the FF did not improve significantly, due to the significantly poorer R_{shunt}. Instead, the superior FF of the modified electrode with a Φ of 5.12 eV resulted from a moderate improvement in balanced contributions from J_{sc}, R_s, and R_{shunt}.

5 Conclusion

In summary we evaluated the performance of a PEDOT:PSS/ITO interface in a polymer-based solar cell, by nanostructuring the ITO surface with sol-LiF nanoparticles covering increasing areal density. We have determined the Φ of the modified ITO by PESA and observed an increase in Φ with increasing coverage of sol-LiF. We have incorporated the modified ITO anodes into anode/PEDOT:PSS/P3HT/PCBM/thermal-LiF/Al BHJ OPVs and compared their performance with non-modified ITO-based control devices. Although the effect of nanostructuring did not significantly perturb wetting of the PEDOT:PSS on the modified ITO surface, the presence of the sol-LiF enabled tuning of the ITO surface Φ, via optimizing coverage of the ITO surface. We conclude that the significantly improved J_{sc} by 84 %, was consistent with an improved electronic hole collection efficiency resulting from optimized energy level alignment between PEDOT:PSS and the modified anode. Furthermore, this optimization is also attributed to lower resistance to charge extraction and improved charge transport balanced by increased contact polarization—*in-operando* IS studies revealed a faster and more efficient collection of mobile holes to the ITO/PEDOT:PSS interface, although polarization of the ITO surface also leads to a higher extraction barrier. Significantly improved recombination resistances, indicating that the hole charge carriers were less likely to recombine within the active layer, may be attributed to more efficient extraction of mobile holes, which would lead to lower hole charge accumulation within the active layer. Our results confirm that sol-LiF can be used to tune the surface Φ of ITO for improved energy level matching with other contact layers and enhance the hole extraction efficiency.

Acknowledgments Financial support is acknowledged from the Scientific and Technological Research Council of Turkey (TUBITAK) for Project No. 112M360, also from H. K. for a BIDEB fellowship. The authors are grateful to Prof. Ayse Turak for fruitful

discussions and to GUNAM at Middle East Technical University for use of their solar simulator.

References

1. B. Kippelen, J.-L. Brédas, Energy Environ. Sci. **2**, 251 (2009)
2. F.C. Krebs, T. Tromholt, M. Jørgensen, Nanoscale **2**, 873 (2010)
3. M.A. Green, K. Emery, Y. Hishikawa, W. Warta, E.D. Dunlop, Prog. Photovolt. Res. Appl. **20**, 12 (2012)
4. R. Søndergaard, M. Hösel, D. Angmo, T.T. Larsen-Olsen, F.C. Krebs, Mater. Today **15**, 36 (2012)
5. H. Ma, H.-L. Yip, F. Huang, A.K.-Y. Jen, Adv. Funct. Mater. **20**, 1371 (2010)
6. G. Li, V. Shrotriya, J. Huang, Y. Yao, T. Moriarty, K. Emery, Y. Yang, Nat. Mater. **4**, 864 (2005)
7. E. Ratcliff, B. Zacher, N. Armstrong, J. Phys. Chem. Lett. **2**, 1337 (2011)
8. J.S. Kim, J.H. Park, J.H. Lee, J. Jo, D.-Y. Kim, K. Cho, Appl. Phys. Lett. **91**, 112111 (2007)
9. M. Gliboff, H. Li, K.M. Knesting, A.J. Giordano, D. Nordlund, G.T. Seidler, J.-L. Brédas, S.R. Marder, D.S. Ginger, J. Phys. Chem. C **117**, 15139 (2013)
10. M. Gliboff, L. Sang, K.M. Knesting, M.C. Schalnat, A. Mudalige, E.L. Ratcliff, H. Li, A.K. Sigdel, A.J. Giordano, J.J. Berry, D. Nordlund, G.T. Seidler, J.-L. Brédas, S.R. Marder, J.E. Pemberton, D.S. Ginger, Langmuir **29**, 2166 (2013)
11. M.G. Helander, Z.B. Wang, J. Qiu, M.T. Greiner, D.P. Puzzo, Z.W. Liu, Z.H. Lu, Science **332**, 944 (2011)
12. C.-Y. Li, T.-C. Wen, T.-F. Guo, J. Mater. Chem. **18**, 4478 (2008)
13. B. Kang, L.W. Tan, S.R.P. Silva, Appl. Phys. Lett. **93**, 133302 (2008)
14. Y. Zhou, C. Fuentes-Hernandez, J. Shim, J. Meyer, A.J. Giordano, H. Li, P. Winget, T. Papadopoulos, H. Cheun, J. Kim, M. Fenoll, A. Dindar, W. Haske, E. Najafabadi, T.M. Khan, H. Sojoudi, S. Barlow, S. Graham, J.-L. Brédas, S.R. Marder, A. Kahn, B. Kippelen, Science **336**, 327 (2012)
15. I.P. Murray, S.J. Lou, L.J. Cote, S. Loser, C.J. Kadleck, T. Xu, J.M. Szarko, B.S. Rolczynski, J.E. Johns, J. Huang, L. Yu, L.X. Chen, T.J. Marks, M.C. Hersam, J. Phys. Chem. Lett. **2**, 3006 (2011)
16. S. Chaudhary, H. Lu, A.M. Müller, C.J. Bardeen, M. Ozkan, Nano Lett. **7**, 1973 (2007)
17. V. Shrotriya, G. Li, Y. Yao, C.-W. Chu, Y. Yang, Appl. Phys. Lett. **88**, 073508 (2006)
18. M.D. Irwin, D.B. Buchholz, A.W. Hains, R.P.H. Chang, T.J. Marks, Proc. Natl. Acad. Sci. **105**, 2783 (2008)
19. K.X. Steirer, P.F. Ndione, N.E. Widjonarko, M.T. Lloyd, J. Meyer, E.L. Ratcliff, A. Kahn, N.R. Armstrong, C.J. Curtis, D.S. Ginley, J.J. Berry, D.C. Olson, Adv. Energy Mater. **1**, 813 (2011)
20. W.-J. Yoon, P.R. Berger, Appl. Phys. Lett. **92**, 013306 (2008)
21. H.-L. Yip, S.K. Hau, N.S. Baek, A.K.-Y. Jen, Appl. Phys. Lett. **92**, 193313 (2008)
22. A. Turak, RSC Adv. **3**, 6188 (2013)
23. L.S.C. Pingree, B.A. MacLeod, D.S. Ginger, J. Phys. Chem. C **112**, 7922 (2008)
24. H. Yan, P. Lee, N.R. Armstrong, A. Graham, G.A. Evmenenko, P. Dutta, T.J. Marks, J. Am. Chem. Soc. **127**, 3172 (2005)
25. K.W. Wong, H.L. Yip, Y. Luo, K.Y. Wong, W.M. Lau, K.H. Low, H.F. Chow, Z.Q. Gao, W.L. Yeung, C.C. Chang, Appl. Phys. Lett. **80**, 2788 (2002)
26. G. Garcia-Belmonte, A. Guerrero, J. Bisquert, J. Phys. Chem. Lett. **4**, 877 (2013)
27. G. Garcia-Belmonte, A. Munar, E.M. Barea, J. Bisquert, I. Ugarte, R. Pacios, Org. Electron. **9**, 847 (2008)
28. T. Aytun, A. Turak, I. Baikie, G. Halek, C.W. Ow-Yang, Nano Lett. **12**, 39 (2012)
29. A. Turak, T. Aytun, C.W. Ow-Yang, Appl. Phys. Lett. **100**, 253303 (2012)
30. C.W. Ow-Yang, J. Jia, T. Aytun, M. Zamboni, A. Turak, K. Saritas, Y. Shigesato, Thin Solid Films **559**, 58 (2014)
31. C.A. Schneider, W.S. Rasband, K.W. Eliceiri, Nat. Methods **9**, 671 (2012)
32. A.S. Bondarenko, G.A. Ragoisha, in *Progress in Chemometrics Research*, ed. by A.L. Pomerantsev (Nova Science Publishers, New York, 2005), p. 89
33. S. Suckow, T.M. Pletzer, H. Kurz, Prog. Photovolt. Res. Appl. **22**, 494 (2014)
34. E.L. Ratcliff, J. Meyer, K.X. Steirer, N.R. Armstrong, D. Olson, A. Kahn, Org. Electron. **13**, 744 (2012)
35. O. Bubnova, Z.U. Khan, H. Wang, S. Braun, D.R. Evans, M. Fabretto, P. Hojati-Talemi, D. Dagnelund, J.-B. Arlin, Y.H. Geerts, S. Desbief, D.W. Breiby, J.W. Andreasen, R. Lazzaroni, W.M. Chen, I. Zozoulenko, M. Fahlman, P.J. Murphy, M. Berggren, X. Crispin, Nat. Mater. **13**, 190 (2014)
36. T. Aernouts, W. Geens, J. Poortmans, P. Heremans, S. Borghs, R. Mertens, Thin Solid Films **403–404**, 297 (2002)
37. C. Waldauf, M.C. Scharber, P. Schilinsky, J.A. Hauch, C.J. Brabec, J. Appl. Phys. **99**, 104503 (2006)
38. T. Strobel, C. Deibel, V. Dyakonov, Phys. Rev. Lett. **105**, 266602 (2010)
39. A. Wagenpfahl, C. Deibel, V. Dyakonov, IEEE J. Sel. Top. Quantum Electron. **16**, 1759 (2010)